Published in final edited form as:
Neurochem Int. 2023 January ; 162: 105441. doi:10.1016/j.neuint.2022.105441.

Efficacy of novel SPAK inhibitor ZT-1a derivatives (1c, 1d, 1g & 1h) on improving post-stroke neurological outcome and brain lesion in mice

Mohammad Iqbal H. Bhuiyan[a,b,c,d], **Sydney Fischer**[a,b], **Shivani M. Patel**[a,b], **Helena Oft**[a,b], **Ting Zhang**[e], **Lesley M. Foley**[f], **Jinwei Zhang**[g], **T. Kevin Hitchens**[f,h], **Bradley J. Molyneaux**[i], **Xianming Deng**[e], **Dandan Sun**[a,b,c,*]

[a]Department of Neurology, University of Pittsburgh, Pittsburgh, PA 15213

[b]Pittsburgh Institute for Neurodegenerative Disorders, University of Pittsburgh, Pittsburgh, PA 15260

[c]Veterans Affairs Pittsburgh Health Care System, Geriatric Research, Educational and Clinical Center, Pittsburgh, PA 15213.

[d]Department of Pharmaceutical Sciences, School of Pharmacy, University of Texas at El Paso, El Paso, TX, 79968, USA

[e]State Key Laboratory of Cellular Stress Biology, School of Life Sciences, Xiamen University, Xiamen, Fujian, China

[f]Animal Imaging Center, University of Pittsburgh, Pittsburgh, Pennsylvania, 15203, USA

[g]Institute of Biomedical and Clinical Sciences, University of Exeter Medical School, Hatherly Laboratory, Exeter, UK

[h]Department of Neurobiology, University of Pittsburgh, Pittsburgh, Pennsylvania, 15213, USA

[i]Department of Neurology, Brigham and Women's Hospital, Boston, MA 02115, USA.

Abstract

SPAK inhibitor ZT-1a was previously shown to be neuroprotective in murine ischemic stroke models. In this study, we further examined the efficacy of four ZT-1a derivatives (ZT-1c, -1d, -1g

[*]**Corresponding author:** Dandan Sun, MD, PhD, Department of Neurology. University of Pittsburgh Medical School, 7016 Biomedical Science Tower-3, 3501 Fifth Ave., Pittsburgh, PA 15260, USA, sund@upmc.edu.

Author contribution statement

Conceived and designed the experiments: M.I.H.B and D.S. Performed the experiments: M.I.H.B., S.F., and L.M.F. Analyzed the data: M.I.H.B., S.F., S.M.P. L.M.F., T.K.H and D.S. Contributed reagents/materials/analysis tools/critical reading: H.O., J.Z., K.K., B.J.M., X.D., T.K.H., and D.S. Wrote the paper: M.I.H.B., S.F., S.M.P., H.O., and D. S.

Disclosure / conflict of interest

The authors declare that they have no conflict of interest.

Declaration of competing interest

The authors declare that they have no known competing financial interests or personal relationship that could have appeared to influence the work reported in this paper.

and -1h) on reducing stroke-induced sensorimotor function impairment and brain lesions. Vehicle control (Veh) or ZT-1 derivatives were administered via osmotic pump to adult C57BL/6J mice during 3-21 hours post-stroke. Neurological behavior of these mice was assessed at days 1, 3, 5, and 7 post-stroke and MRI T2WI and DTI analysis was subsequently conducted in ex vivo brains. Veh-treated stroke mice displayed sensorimotor function deficits compared to Sham mice. In contrast, mice receiving ZT-1a derivatives displayed significantly lower neurological deficits at days 3-7 post-stroke ($p < 0.05$), with ZT-1a, ZT-1c and ZT-1d showing greater impact than ZT-1h and ZT-1g. ZT-1a treatment was the most effective in reducing brain lesion volume on T2WI and in preserving $NeuN^+$ neurons ($p < 0.01$), followed by ZT-1d > −1c > −1g > −1h. The Veh-treated stroke mice displayed white matter tissue injury, reflected by reduced fractional anisotropy (FA) or axial diffusivity (AD) values in external capsule, internal capsule and hippocampus. In contrast, only ZT-1a- as well as ZT-1c-treated stroke mice exhibited significantly higher FA and AD values. These findings demonstrate that post-stroke administration of SPAK inhibitor ZT-1a and its derivatives (ZT-1c and ZT-1d) is effective in protecting gray and white matter tissues in ischemic brains, showing a potential for ischemic stroke therapy development.

Keywords

DTI; Ischemic Stroke; MRI; Neurodegeneration; Neuroprotection; SPAK; MRI-detected brain lesion

1. INTRODUCTION

Stroke is the fifth leading cause of death (with 3.3 million deaths per year) and affects 77.2 million people globally each year (Virani et al, 2021). An infarction in the brain, spinal cord, or retina after stroke leads to a corresponding loss of neurologic function (Campbell et al, 2019), which carries a significant economic burden; approximately 34% of global total healthcare costs are spent on stroke, with $33 billion in annual costs (Rochmah et al, 2021). Currently, two primary therapeutic strategies are available for acute ischemic stroke patients: recombinant tissue plasminogen activator (tPA) and endovascular thrombectomy (Bhatia et al, 2020). However, only 8-15% of acute ischemic stroke patients are eligible for these treatments due to several factors, including their narrow treatment time window (Kleindorfer et al, 2013; Smith et al, 2017). Moreover, administration of tPA beyond 4.5 hours post-stroke causes significant increase in hemorrhagic transformation compared to the placebo group (Maier et al, 2020). Thus, development of novel neuroprotective agents for ischemic stroke is urgently needed.

Evolutionary conserved WNK [“with no lysine” (K)] kinases and the downstream SPAK/OSR1 (Ste20/SPS1-related proline/alanine-rich kinase and oxidative stress-responsive kinase 1) kinases regulate activities of multiple ion transporters/channels and are abundantly expressed in brain cells (Gagnon et al, 2013; Piechotta et al, 2003; Wang et al, 2022). Recent research findings from our studies as well as others’ suggested a critical role of WNK-SPAK/OSR1-NKCC1 signaling in several neurological diseases including ischemic stroke and post-hemorrhagic hydrocephalus (Bhuiyan et al, 2017; Brown et al, 2021; Huang et al, 2019; Zhao et al, 2017). Ischemic stroke triggers upregulation of WNK-SPAK/OSR1

kinases in ischemic brains, which contributes to ischemia-induced brain damage (Begum et al, 2015; Huang et al, 2019; Zhao et al, 2017). Therefore, in a recent study, we designed and synthesized 10 novel non-ATP-competitive SPAK-specific inhibitors (Zhang et al, 2020). The lead compound ZT-1a with EC50 μ1 μM on inhibiting the cellular SPAK activity was shown to penetrate ischemic stroke mouse brain administered at 3 hours after reperfusion (Zhang et al, 2020) and attenuate neuronal death in both transient and permanent ischemic stroke models (Bhuiyan et al, 2022; Zhang et al, 2020). Among these 10 novel SPAK inhibitors, ZT-1a derivatives ZT-1 “c”, “d”, “g”, and “h” share chemical structures of ZT-1a and displayed similar SPAK kinase inhibition activities in *in vitro* study with EC50 of 3 μM (Zhang et al, 2020). However, the efficacy of these ZT-1a derivatives in reducing ischemic stroke-mediated brain injury has not been evaluated in vivo. In this study, using the well-established middle cerebral artery occlusion (MCAO) ischemic stroke model in adult C57BL/6J mice, we assessed effects of ZT-1 derivatives “a”, “c”, “d”, “g”, and “h” in reducing ischemic stroke-mediated brain injury and neurological deficits. The new study demonstrated that post-stroke administration of SPAK inhibitor ZT-1a or its derivatives (ZT-1c and ZT-1d) is effective in protecting gray and white matter tissues in ischemic brains, showing their potentials for ischemic stroke therapy development.

2. Materials and methods

2.1. Animal preparation

All animal experiments were approved by the University of Pittsburgh Institutional Animal Care and Use Committee and performed in accordance with the National Institutes of Health Guide for the Care and Use of Laboratory Animals. This manuscript adheres to the ARRIVE guidelines for reporting animal experiments. Nine- to 14-week-old C57BL/6J male mice (Jackson laboratories, Bar Harbor, ME) were used in the study.

2.2. Transient middle cerebral artery occlusion model (t-MCAO)

Focal cerebral ischemia was induced by transient occlusion of the left middle cerebral artery (MCA) for 50 min as described previously (Bhuiyan et al, 2022; Zhang et al, 2020). Briefly, under an operating microscope, the left common carotid artery was exposed through a midline incision. Two branches of the external carotid artery (ECA), occipital and superior thyroid arteries, were isolated and coagulated. The ECA was dissected further distally and permanently ligated. The internal carotid artery (ICA) was isolated and carefully separated from the adjacent vagus nerve. A 12 mm length of silicon- coated nylon filament (size 6-0, native diameter 0.11 mm; diameter with coating 0.20+/− 0.02 mm; coating length 4-5 mm; Doccol Corporation, Sharon, MA) was introduced into the ECA lumen through a puncture. The silk suture around the ECA stump was tightened around the intraluminal nylon suture to prevent bleeding. The nylon suture was then gently advanced from the ECA to the ICA lumen until mild resistance was felt (~9 mm). For reperfusion, the suture was withdrawn 50 min after MCAO to restore blood flow. Body temperature was maintained for the duration of the experiment between 36.5-37.0 °C with a small animal heating pad (Kent Scientific).

2.3. Drug treatment

Mice were randomly assigned to receive either Veh (50% DMSO in PBS, 2 ml/kg body weight/day) or ZT-1a-derivatives (1a, 1c, 1d, 1g and 1h; 5.0 mg/kg body weight/day) at 3-21 hours after reperfusion via continuous infusion subcutaneously (s.c.) by osmotic minipump (model 2001D, Alzet, Figure 1A).

2.4. Neurological function deficit assessment

Neurological function scoring: Neurological functional deficits in mice were assessed in a blinded manner with two assessment scales at 1, 3, 5, and 7 days after t-MCAO. These tests are established for identifying and quantifying sensorimotor deficits and postural asymmetries on a scale of 0 to 4 as previously described (Huang et al, 2019). Scores are assigned accordingly: 0=no observable deficit, 1=forelimb flexion, 2=forelimb flexion and decreased resistance to lateral push, 3=forelimb flexion, decreased resistance to lateral push, and unilateral circling, and 4=forelimb flexion and being unable/difficult to ambulate (Schaar et al, 2010; Zhang et al, 2002).

Adhesive tape removal test: An adhesive tape removal test was used to measure somatosensory deficits as described by Bhuiyan et al (2022). The contact time of adhesive tape (3mm by 4mm) from the right forepaw is defined as the time at which the animal contacts the tape with its mouth. The removal time of an adhesive tape from the right forepaw is defined as the time at which the animal removes the tape. The trial ends after the adhesive patch is removed, or after 2 min have elapsed. Pre-operative training was carried out once per day for three days (Zhao et al, 2017).

Grid walking foot-fault test: The grid walking test is sensitive to deficits in descending motor control. Each mouse was placed on a stainless-steel grid floor (20×40 cm with a mesh size of 4 cm^2) elevated 1 m above the floor. Every animal was tested with at least 50 steps per trial. Prior to ischemic stroke, the mice were placed on the grid to establish a baseline. The data was expressed as the number of foot fault errors made by the forelimbs contralateral to the injured hemisphere as a percentage of total steps (Zhang et al, 2017).

Cylinder test: The cylinder test was carried out to evaluate asymmetry of forelimb use. Mice were placed in a transparent cylinder (9 cm in diameter and 15 cm in height) for 10 min and all the forelimb movements of the mice were recorded by a camera fixed above the cylinder. Forepaw (left/right/both) usage on initial contact against the cylinder wall after rearing and during lateral exploration was counted. If both forepaws were used during rearing and the impaired forelimb slipped, then only the non-impaired forelimb was counted. Preference of the impaired forepaw was calculated such that the final score was determined based on the following formula: (non-impaired forelimb movement –impaired forelimb movement)/(non-impaired forelimb movement + impaired forelimb movement + both forelimb movement). Prior to ischemic stroke, animals were placed in the cylinder for 5 min to establish a baseline symmetry profile. If any animals showed behavioral asymmetries, they were excluded from further analysis (Zhang et al, 2017).

Corner test: The corner test was carried out to evaluate asymmetry of motor capabilities. An apparatus was used to create a 30° angle for the corner as described by Zhao et al (2017). There were 10 trials for each test with the mouse either making a left or right turn. The rearing movement is necessary for the turn to be scored. The scoring was determined by |(left turn – right turn)| as affected mice will show asymmetrical favoritism to either side.

2.5. Magnetic Resonance Imaging (MRI) T_2-weighted images (T2WI) and diffusion tensor imaging (DTI) of ex vivo brains

After completion of the neurological function assessment at day 7 post-stroke, the cohort of mice were anesthetized with 5% isoflurane, transcardially perfused with 0.1 M PBS (pH 7.4), followed by ice-cold 4% paraformaldehyde (PFA) in 0.1 M PBS, and decapitated, as described previously (Zhang et al, 2020). Ex vivo brains were maintained within the skull to avoid anatomical deformation. After post-fixation in 4% PFA overnight, heads were stored in a PBS solution at 4° C. MRI was performed at 500 MHz using a Bruker AV3HD 11.7 T/89 mm vertical bore small animal MRI scanner, equipped with a 20-mm quadrature radiofrequency (RF) coil and ParaVision 6.0.1 software (Bruker Biospin, Billerica, MA). Following positioning and pilot scans, T2-weighted images, T2WI were acquired using a Rapid Acquisition with Relaxation Enhancement (RARE) sequence, with the following parameters: Echo Time/Time of Repetition (TE/ TR) of 20/3500 ms, 2 averages, 256 x 256 matrix, 25 slices with a 1 mm slice thickness, a RARE factor of 4, and a field of view (FOV) of 22 x 22 mm. A DTI dataset covering the entire brain was collected using a multi-slice spin echo sequence with 3 A0 and 30 non-collinear diffusion-weighted images with the following parameters: TE/TR = 22/5000 ms, 4 averages, matrix size = 192 × 192 reconstructed to 256 × 256, FOV = 22 × 22 mm, 25 axial slices, slice thickness = 1 mm, b-value = 1200 s/mm^2, and Δ/δ = 10/5 ms. DTI and T2 datasets were analyzed with DSI Studio (http://dsi-studio.lab-solver.org/). In a blinded manner, region of interests (ROIs) was drawn in 10 axial slices (covering +1.92 mm to −3.52 mm posterior from the bregma) segmenting the corpus callosum (CC), external capsule (EC), internal capsule (IC), and hippocampus (HP) and T2 lesion area in both the ipsilateral and contralateral hemispheres. DSI software provided total T2 lesion volume of ipsilateral hemisphere, while fractional anisotropy (FA) values and axial diffusivity (AD) values for the CC, EC, IC, and HP were obtained for each mouse brain before the means and standard errors were determined for all animals in each group.

2.6. Immunofluorescence staining

Immunofluorescent staining for neuronal nuclei (NeuN) was performed as described previously (Bhuiyan et al, 2017). Post MRI study, brain sections at three different levels (0.62 mm, −0.34 mm, −1.1 mm posterior from the bregma) from each brain were selected and processed for immunofluorescent staining. The sections were incubated with blocking solution (10% normal goat serum, 3% bovine serum albumin, and 0.15% Triton X-100 in PBS) for 1 h at room temperature and were then incubated with anti-NeuN antibody (1:200) in the blocking solution for overnight at 4 °C. After washing in TBS for 3×10 min, the sections were incubated with goat anti-rabbit Alexa 488-conjuagated IgG (1:200, Thermo Fisher Scientific) in the blocking solution for 1 h. For negative controls, brain sections were stained with the secondary antibodies only. After washing for 3 times, nuclei were

stained with DAPI (1:1000, Thermo Fisher Scientific) for 20 min at 37 °C. Sections were mounted with Vectashield mounting medium (Vector Laboratories). Fluorescent images were captured under 4× lens using an Olympus Ix83 inverted microscope. The ischemic area for each slice was calculated by subtracting the non-infarct area in the IL hemisphere from the total area of the contralateral CL hemisphere using NIH ImageJ software. The average infarct area (mm^2) of three sections was multiplied by 1.7 mm (total thickness of the measured brain) to calculate infarct volume (mm^3) for each mouse brain before the means and standard errors were determined for all animals in each group.

2.7. Statistics

Animal subjects were randomly assigned to different treatment groups and surgical procedures. All data analyses were performed by investigators blinded to experimental conditions. The number of animals studied was 80% powered to detect 25% changes with α (2-sided) = 0.05. A total of 45 male mice were used in the study. All mice were included in the study except 6 mice which died during stroke surgery (2) or during treatment in veh (2), 1c (1) and 1g (1) group. Twelve ex vivo brains were excluded from the DTI analysis due to a fixation artifact including a hyper-intense rim around the brain with reduced gray-white matter contrast inversion due to less optimal perfusion of PFA (Cahill et al, 2012). Data were expressed as mean ± SEM. Statistical significance was determined by two-way ANOVA using the Tukey's post-hoc test for multiple comparisons (GraphPad Prism 6.0, San Diego, CA, USA). A probability value < 0.05 was considered statistically significant.

3. RESULTS

3.1. Comparison of effects of ZT-1a and its derivatives on improving neurological outcome in stroke mice

We first assessed efficacy of the lead SPAK inhibitor ZT-1a and its four derivative drugs (ZT-1c, ZT-1d, ZT-1g, and ZT-1h) on improving neurological functional recovery on day 1, 3, 5, and 7 post-stroke using the transient MCAO model (Fig. 1). Compared to Sham group, ischemic stroke led to a moderate body weight loss (14.8 −25.9 %, $p < 0.05$) in the Veh- and drug-treated groups at 3-7 days after tMCAO (Fig. 1B). There were no significant differences in body weight changes between the Veh-treated and the ZT-1a- and four derivatives-treated mice (Fig. 1B). However, analysis of the neurological scores, a composite index for neurological function deficits in motor skills, revealed that ZT-1a and ZT-1d-treatment significantly accelerated post-stroke neurological function recovery at day 7 (* $p< 0.05$ compared to day 1), whereas, the Veh-, ZT-1c-, ZT-1g- or ZT-1h-treated mice did not show neurological function improvement at day 7 compared to day 1 (Fig. 1C). ZT-1a-treated mice showed better neurological function compared to Veh group at days 5 and 7 post-stroke (# $p <0.05$ vs. Veh; Fig. 1C). In assessing unilateral movement behaviors of these mice in the corner test and cylinder test (Fig. 1D-E) stroke caused asymmetric motor movement in the Veh- and five drug-treated stroke mice, compared to Sham mice. The Veh-treated mice displaying the most consistent lack of symmetry in movement in day 1-7 post-stroke. All five drug-treated mice showed a decline in scoring in the cylinder test (Fig. 1E), indicating an improvement in forelimb motor function, but only ZT-1a treatment group displayed significantly better outcomes at 1–5-day post-stroke compared to

the Veh-treated group (# $p < 0.05$). Interestingly, all five ZT-1 derivative drugs-treated stroke mice exhibited significantly less foot missteps or faster sensory-motor function recovery in the foot-fault test, and adhesive contact test compared to Veh-treated stroke mice ($^{\&}$ and $^{\#}p < 0.05$; Fig. 1F-G). ZT-1a and its four derivatives demonstrated different degrees of efficacy in improving neurological function. Notably, derivatives improved sensorimotor function in the foot-fault and adhesive tape contact tests and were less effective in improving asymmetry movement deficits. Taken together, ZT-1a is the most efficacious in improving stroke-induced neurological function deficits followed by ZT-1d > −1c > −1g > −1h.

3.2. Comparison of effects of ZT-1a and its derivatives on decreasing brain lesion volume in stroke mice

After completion of the neurological function assessments of the cohort described in Fig. 1, MRI acquisition was subsequently performed ex vivo. Fig. 2A illustrates representative T2-weighted images (T2WI) of Sham, Veh-treated, ZT-1a- or derivative-treated brains, where the white dotted lines indicate boundaries of the stroke lesions. Quantitative analysis showed that ZT-1a as well as the four derivatives (1d, 1c, 1g, or 1h) reduced stroke-lesion volume by ~ 65.2%, 55.1%, 46.5%, 40.6%, or 25.6%, respectively (Fig. 2A and B). ZT-1a and ZT-1d exhibited significantly better protection than ZT-1h ($p < 0.05$). The neuroprotective effects detected with T2WI analysis were further corroborated by immunofluorescence staining of $NeuN^+$ cells (Fig. 2C). Loss of $NeuN^+$ staining in the stroke infarct region was most pronounced in the Veh-treated mice (Fig. 2C), and ZT-1a and its four derivatives showed different degrees of neuroprotection. ZT1-a, ZT-1d and ZT-1c showed significant reduction of infarct volume by 52.0%, 39.4%, and 38.1%, respectively ($p < 0.01$), while effects of ZT-1g and ZT-1h did not reach statistical significance ($p > 0.05$, Fig. 2C and D). Cumulatively these results further suggest that ZT-1a and its derivative ZT-1c and ZT-1d are indeed neuroprotective and preserve $NeuN^+$ neurons in ischemic brains.

3.3. Effects of ZT-1a and its derivatives on preserving white matter integrity following stroke

We also performed DTI on the ex vivo brains to investigate white matter integrity changes of corpus callosum (CC), external capsule (EC), internal capsule (IC), and hippocampus (HP). Representative directionally encoded color (DEC) maps of each brain were shown in Fig. 3A and 4A. The CL hemisphere DEC map of the Veh-treated stroke brain shows intact CC, EC, IC, and HP tracks (**arrowhead**), however, the IL hemisphere displayed injured EC, IC or HP (**arrow**). Compared to the CL hemisphere, analysis of fractional anisotropy (FA) and axial diffusivity (AD) revealed a significant reduction of FA and AD values in the IL EC as well as IC tracts of the Veh-treated, and four derivative-treated mice, reflecting loss of white matter microstructure integrity after stroke (Fig. 3B). However, ZT-1a treatment prevented stroke-induced decreases in FA and AD values of the EC and IC regions, and mostly preserved FA and AD in the CC (Fig. 3B). Interestingly, ZT-1c or ZT-1g showed occasional increased protection when compared to Veh-treated animals in the AD values of the EC, IC and CC and the FA values of the CC. However, except ZT-1a, none of the four derivatives is effective in preventing white matter integrity in HP, reflected by decreases of FA values (Fig. 4B). Taken together, our unbiased DTI MRI analysis suggests that post-stroke administration of ZT-1a and its derivatives ZT-1c and ZT-1d were robust in protecting gray matter tissue in

ischemic brains. However, only ZT-1a and ZT-1c constantly illustrated protective effects in preserving white matter integrity.

4. DISCUSSION

Stroke-induced activation of WNK-SPAK-NKCC1 signaling complex in ischemic brains

SPAK kinase is ubiquitously expressed in both the murine and human brain and enriched in neurons, astrocytes, oligodendrocytes and choroid plexus epithelial cells (Gagnon and Delphire, 2013; Murillo-de-Ozores et al, 2020). In the healthy brain, the WNK-SPAK/OSR1-NKCC1 pathway is a key regulator of cell volume and fluid homeostasis (Brown et al, 2021). The pathway also functions to modulate Cl^- homeostasis by increasing Cl^- influx through activating NKCC1 and decreasing Cl^- efflux through inhibiting KCC 1-4, respectively (Zhang et al, 2020). Ischemic stroke events trigger phosphorylation and activation of WNK in ischemic brains, leading to phosphoactivation of SPAK and/or OSR1 and NKCC1 protein and contributing to cerebral edema, neuronal and glial cell death during the first 24 hours after stroke injury (Bhuiyan et al, 2017, 2022; Huang et al, 2019; Zhang et al, 2020). Ischemic stroke also activates the WNK-SPAK/OSR1-NKCC1 cascade at the transcriptional level in part via NF-kB signaling, which subsequently upregulates WNK, SPAK and NKCC1 gene and protein expression (Bhuiyan et al, 2017, 2022; Huang et al, 2019; Zhang et al, 2020). Post-stroke administration of ZT-1a in mice decreases SPAK kinase phosphorylation and reduces infarct size and neurological function deficits ((Bhuiyan et al, 2022; Zhang et al, 2020). While these findings from experimental animal models of stroke suggest this signaling pathway as a highly promising new target for stroke therapy, it remains to be explored clinically.

Different efficacy of ZT-1a and the four derivatives in reducing stroke-induced brain injury

Previously, we synthesized the novel SPAK inhibitor ZT-1a using a “scaffold-hybrid” strategy which combines moieties from other known SPAK inhibitors to block the kinase’s activation by WNK (Bhuiyan et al, 2022; Zhang et al, 2020). Association of ZT-1a and its derivatives with WNK and their ability to inhibit SPAK-dependent phosphorylation have been validated *in vitro* (Zhang et al, 2020). This study is the first to assess the impact of ZT-1a derivatives (ZT-1c, 1d, 1g and 1h) on improving neurological function deficit, stroke lesion volume as well as gray vs. white matter tract integrity. In our previous study, we reported that intravenous administration of ZT-1a in naïve mice shows pharmacokinetics with $T_{1/2}$ (plasma half life) = 1.8 hours, AUC (area under the curve) =2340 hours*ng/mL, MRT (mean residence time) = 0.45 hours, while an oral dose shows $T_{1/2}$ = 2.6 hours, AUC =97.3 hours*ng/mL, MRT = 3.3 hours, and 2.2% oral bioavailability (Zhang et al, 2020). We also found that early inhibition of SPAK in mouse brains (ZT-1a administration at 3 hours and 8 hours after stroke) showed neuroprotection detected at 24 hours and at 7 days after stroke (sustained protective effects; Zhang et al, 2020; Bhuiyan et al, 2022). As four derivatives ZT-1c, 1d, 1g and 1h shared nearly identical chemical structure and physical properties (lipophilicity, surface polar area, etc.) to ZT-1a and demonstrated similar cellular SPAK inhibitory activities *in vitro*, we assume that these four derivatives may also have similar short $T_{1/2}$. Therefore, to maintain a constant plasma concentration and to inhibit SPAK at the initial 3-21 hours after stroke, we employed osmotic pump (Wang-

Fischer, Manual of Stroke Models in Rats, 2008) to deliver ZT-1a and the four derivatives subcutaneously. Osmotic pump delivered derivatives at a consistent rate (3.5 μg/kg/min) over 3-21 hours post-stroke. With this dose regimen, ZT-1c, 1d, 1g and 1h exhibited a range of neuroprotective capacity across behavioral tests and lesion imaging, though only ZT-1a significantly improved neurological function in all tests. Among four derivatives, ZT-1c and ZT-1d demonstrated most promising trends in improving neurologic functional recovery (in the foot fault and adhesive contact tests) and preserving gray and white matter after ischemic injury.

Derivatives ZT-1g and −1h also reduced deficits in foot fault and adhesive contact tests and displayed some improvement in lesion volume on MRI but did not show significant effects on either reducing $NeuN^+$ neuronal loss or white/grey matter damage on FA or AD values (Fig. 1-4). Only ZT1-a treatment showed increases in either FA or AD for EC and CC, whereas ZT-1c significantly improved the AD values of the EC and IC. The cause(s) for the apparent different efficacies between ZT-1a and four derivatives are not known. Our previous SPAK kinase inhibition capacity study shows that ZT-1a achieved 50% inhibition of SPAK (pSer373) at 1μM while its derivatives (ZT-1c, 1d, 1g and 1h) do so at 3μM (Zhang et al, 2020). However, the EC50s for inhibition of SPAK, NKCC1 and KCC3 are identical across derivatives as are their approximate, calculated lipophilicity and total polar surface areas (Tetko and Tanchuk, 2002; Tetko et al, 2005). Possible mechanisms for the different effects of these similar compounds could be further clarified by examining their distinct pharmacokinetics, including exact concentration and activity level in stroke tissues. For instance, rates at which these derivatives get into the CNS are likely altered in this context given the breakdown of the BBB in stroke brains (Knowland et al, 2014; Nian et al, 2020; Zhang et al, 2020). Finally, the inconsistent outcomes between behavioral tests and range of infarct volume reduction may arise from the small sample size per group with observed variability in our multiple group comparisons. Future studies with a larger sample size and fewer novel treatment arms would increase statistical power, lower the probability of missing a true difference in outcomes, and allow us to define more subtle differences between groups with greater accuracy (Serdar et al, 2020).

5. CONCLUSION

Ischemic stroke triggered upregulation of WNK-SPAK/OSR1-NKCC1 signaling complex, which contributes to ischemia-induced brain damage. Our recent study reported that a newly developed, potent SPAK inhibitor ZT-1a is neuroprotective against ischemic stroke (Bhuiyan et al, 2022; Zhang et al, 2020). Here we assessed the efficacy of four ZT-1a derivatives (ZT-1c, 1d, 1g and 1h) and demonstrated that continuous administration of ZT-1c and ZT-1d at 3-21 hours post-stroke accelerated neurological functional recovery, with ZT-1c treatment significantly protecting both gray and white matter brain tissue in mice. These new findings further cement ZT-1a and now ZT-1c and ZT-1d as highly promising candidates for future neuroprotective drug development.

Funding sources

This work was supported by Veteran Affairs grants VA I01BX002891-01A1 (D.S.), IK6 BX005647 (D.S.) and NIH grant R01 NS166199-01A1 (M.I.H.B.), and The Royal Society UK IEC\NSFC\201094 (J.Z.).

Abbreviations and Acronyms:

AD	axial diffusivity
CC	corpus callosum
CL	contralateral
DTI	diffusion tensor imaging
EC	external capsule
FA	fractional anisotropy
IC	internal capsule
IL	ischemic ipsilateral
MRI	magnetic resonance imaging
NKCC1	Na-K-Cl cotransporter 1
OSR1	oxidative stress-responsive kinase 1
SPAK	STE20/SPS1-related proline/alanine-rich kinase
tMCAO	Transient occlusion of the middle cerebral artery
Veh	vehicle
WNK	with no lysine (K) kinases

REFERENCES

1. Bhatia K, Bhagavan S, Bains N, French B, Siddiq F, Gomez CR, Qureshi AF, 2020. Current Endovascular Treatment of Acute Ischemic Stroke. Mo Med 117, 480–489. [PubMed: 33311759]
2. Bhuiyan MIH, Song S, Yuan H, Begum G, Kofler J, Kahle KT, Yang S-S, Lin S-H, Alper SL, Subramanya AR, Sun D, 2017. WNK-Cab39-NKCC1 signaling increases the susceptibility to ischemic brain damage in hypertensive rats. J Cereb Blood Flow Metab 37, 2780–2794. 10.1177/0271678X16675368 [PubMed: 27798271]
3. Bhuiyan MIH, Young CB, Jahan F, Hasan MN, Fischer S, Meor Azlan NF, Liu M, Chattopadhyay A, Huang H, Kahle KT, Zhang J, Poloyac SM, Molyneaux BJ, Straub AC, Deng X, Gomez D, Sun D, 2022. NF-κB Signaling-Mediated Activation of WNK-SPAK-NKCC1 Cascade in Worsened Stroke Outcomes of Ang II–Hypertensive Mice. Stroke 53, 1720–1734. 10.1161/STROKEAHA.121.038351 [PubMed: 35272484]
4. Brown A, Meor Azlan NF, Wu Z, Zhang J, 2021. WNK-SPAK/OSR1-NCC kinase signaling pathway as a novel target for the treatment of salt-sensitive hypertension. Acta Pharmacol Sin 42, 508–517. 10.1038/s41401-020-0474-7 [PubMed: 32724175]
5. Cahill LS, Laliberté CL, Ellegood J, Spring S, Gleave JA, van Eede MC, Lerch JP, Henkelman RM, 2012. Preparation of fixed mouse brains for MRI. Neuroimage 60, 933–939. 10.1016/j.neuroimage.2012.01.100 [PubMed: 22305951]
6. Campbell BCV, De Silva DA, Macleod MR, Coutts SB, Schwamm LH, Davis SM, Donnan GA, 2019. Ischaemic stroke. Nat Rev Dis Primers 5, 70. 10.1038/s41572-019-0118-8 [PubMed: 31601801]

7. Frontiers | Blood-Brain Barrier Damage in Ischemic Stroke and Its Regulation by Endothelial Mechanotransduction [WWW Document], n.d. URL https://www.frontiersin.org/articles/10.3389/fphys.2020.605398/full (accessed 7.12.22).
8. Gagnon KB, Delpire E, 2013. Physiology of SLC12 transporters: lessons from inherited human genetic mutations and genetically engineered mouse knockouts. American Journal of Physiology-Cell Physiology 304, C693–C714. 10.1152/ajpcell.00350.2012 [PubMed: 23325410]
9. Gagnon KB, Delpire E, 2012. Molecular Physiology of SPAK and OSR1: Two Ste20-Related Protein Kinases Regulating Ion Transport. Physiological Reviews 92, 1577–1617. 10.1152/physrev.00009.2012 [PubMed: 23073627]
10. Huang H, Bhuiyan MIH, Jiang T, Song S, Shankar S, Taheri T, Li E, Schreppel P, Hintersteininger M, Yang S-S, Lin S-H, Molyneaux BJ, Zhang Z, Erker T, Sun D, 2019. A Novel Na^+-K^+-Cl^- Cotransporter 1 Inhibitor STS66* Reduces Brain Damage in Mice After Ischemic Stroke. Stroke 50, 1021–1025. 10.1161/STROKEAHA.118.024287 [PubMed: 30862257]
11. Josiah SS, Meor Azlan NF, Zhang J, 2021. Targeting the WNK-SPAK/OSR1 Pathway and Cation-Chloride Cotransporters for the Therapy of Stroke. Int J Mol Sci 22, 1232. 10.3390/ijms22031232 [PubMed: 33513812]
12. Kleindorfer D, de los Rios La Rosa F, Khatri P, Kissela B, Mackey J, Adeoye O, 2013. Temporal Trends in Acute Stroke Management. Stroke 44. 10.1161/STROKEAHA.113.001457
13. Knowland D, Arac A, Sekiguchi KJ, Hsu M, Lutz SE, Perrino J, Steinberg GK, Barres BA, Nimmerjahn A, Agalliu D, 2014. Stepwise Recruitment of Transcellular and Paracellular Pathways Underlies Blood-Brain Barrier Breakdown in Stroke. Neuron 82, 603–617. 10.1016/j.neuron.2014.03.003 [PubMed: 24746419]
14. Maïer B, Desilles JP, Mazighi M, 2020. Intracranial Hemorrhage After Reperfusion Therapies in Acute Ischemic Stroke Patients. Frontiers in Neurology https://www.frontiersin.org/articles/10.3389/fneur.2020.599908.
15. Murillo-de-Ozores AR, Chávez-Canales M, de los Heros P, Gamba G, Castañeda-Bueno M, 2020. Physiological Processes Modulated by the Chloride-Sensitive WNK-SPAK/OSR1 Kinase Signaling Pathway and the Cation-Coupled Chloride Cotransporters. Frontiers in Physiology 11.
16. Nian K, Harding IC, Herman IM, Ebong EE, 2020. Blood-Brain Barrier Damage in Ischemic Stroke and Its Regulation by Endothelial Mechanotransduction. Frontiers in Physiology 11.
17. Piechotta K, Garbarini N, England R, Delpire E, 2003. Characterization of the Interaction of the Stress Kinase SPAK with the Na+-K+-2Cl− Cotransporter in the Nervous System. Journal of Biological Chemistry 278, 52848–52856. 10.1074/ibc.M30943620Q [PubMed: 14563843]
18. Rochmah TN, Rahmawati IT, Dahlui M, Budiarto W, Bilqis N, 2021. Economic Burden of Stroke Disease: A Systematic Review. IJERPH 18, 7552. 10.3390/ijerph18147552 [PubMed: 34299999]
19. Schaar KL, Brenneman MM, Savitz SI, 2010. Functional assessments in the rodent stroke model. Exp & Trans Stroke Med 2, 13. 10.1186/2040-7378-2-13
20. Serdar CC, Cihan M, Yücel D, Serdar MA, 2021. Sample size, power and effect size revisited: simplified and practical approaches in pre-clinical, clinical and laboratory studies. Biochem Med (Zagreb) 31, 010502. 10.11613/BM.2021.010502 [PubMed: 33380887]
21. Smith EE, Saver JL, Cox M, Liang L, Matsouaka R, Xian Y, Bhatt DL, Fonarow GC, Schwamm LH, 2017. Increase in Endovascular Therapy in Get With The Guidelines-Stroke After the Publication of Pivotal Trials. Circulation 136, 2303–2310. 10.1161/CIRCULATIONAHA.117.031097 [PubMed: 28982689]
22. Tetko IV, Gasteiger J, Todeschini R, Mauri A, Livingstone D, Ertl P, Palyulin VA, Radchenko EV, Zefirov NS, Makarenko AS, Tanchuk VY, Prokopenko VV, 2005. Virtual computational chemistry laboratory--design and description. J Comput Aided Mol Des 19, 453–463. 10.1007/s10822-005-8694-y [PubMed: 16231203]
23. Tetko IV, Tanchuk VY, 2002. Application of associative neural networks for prediction of lipophilicity in ALOGPS 2.1 program. J Chem Inf Comput Sci 42, 1136–1145. 10.1021/ci025515j [PubMed: 12377001]
24. Virani SS, Alonso A, Aparicio HJ, Benjamin EJ, Bittencourt MS, Callaway CW, Carson AP, Chamberlain AM, Cheng S, Delling FN, Elkind MSV, Evenson KR, Ferguson JF, Gupta DK, Khan SS, Kissela BM, Knutson KL, Lee CD, Lewis TT, Liu J, Loop MS, Lutsey PL, Ma J,

Mackey J, Martin SS, Matchar DB, Mussolino ME, Navaneethan SD, Perak AM, Roth GA, Samad Z, Satou GM, Schroeder EB, Shah SH, Shay CM, Stokes A, VanWagner LB, Wang N-Y, Tsao CW, On behalf of the American Heart Association Council on Epidemiology and Prevention Statistics Committee and Stroke Statistics Subcommittee, 2021. Heart Disease and Stroke Statistics—2021 Update: A Report From the American Heart Association. Circulation 143. 10.1161/CIR.0000000000000950

25. Wang J, Liu R, Hasan MN, Fischer S, Chen Y, Como M, Fiesler VM, Bhuiyan MIH, Dong S, Li E, Kahle KT, Zhang J, Deng X, Subramanya AR, Begum G, Yin Y, Sun D, 2022. Role of SPAK–NKCC1 signaling cascade in the choroid plexus blood–CSF barrier damage after stroke. J Neuroinflammation 19, 91. 10.1186/s12974-022-02456-4 [PubMed: 35413993]
26. Wang-Fischer Y, 2008. Manual of Stroke Models in Rats. CRC Press.
27. Zhang J, Pu H, Zhang H, Wei Z, Jiang X, Xu M, Zhang L, Zhang W, Liu J, Meng H, Stetler RA, Sun D, Chen J, Gao Y, Chen L, 2017. Inhibition of Na + -K + -2C1 − cotransporter attenuates blood-brain-barrier disruption in a mouse model of traumatic brain injury. Neurochemistry International 111, 23–31. 10.1016/j.neuint.2017.05.020 [PubMed: 28577991]
28. Zhang Jinwei, Bhuiyan MIH, Zhang T, Karimy JK, Wu Z, Fiesler VM, Zhang Jingfang, Huang H, Hasan MN, Skrzypiec AE, Mucha M, Duran D, Huang W, Pawlak R, Foley LM, Hitchens TK, Minnigh MB, Poloyac SM, Alper SL, Molyneaux BJ, Trevelyan AJ, Kahle KT, Sun D, Deng X, 2020. Modulation of brain cation-Cl− cotransport via the SPAK kinase inhibitor ZT-1a. Nat Commun 11, 78. 10.1038/s41467-019-13851-6 [PubMed: 31911626]
29. Zhang L, Schallert T, Zhang ZG, Jiang Q, Arniego P, Li Q, Lu M, Chopp M, 2002. A test for detecting long-term sensorimotor dysfunction in the mouse after focal cerebral ischemia. J Neurosci Methods 117, 207–214. 10.1016/s0165-0270(02)00114-0 [PubMed: 12100987]
30. Zhao H, Nepomuceno R, Gao X, Foley LM, Wang S, Begum G, Zhu W, Pigott VM, Falgoust LM, Kahle KT, Yang S-S, Lin S-H, Alper SL, Hitchens TK, Hu S, Zhang Z, Sun D, 2017. Deletion of the WNK3-SPAK kinase complex in mice improves radiographic and clinical outcomes in malignant cerebral edema after ischemic stroke. J Cereb Blood Flow Metab 37, 550–563. 10.1177/0271678X16631561 [PubMed: 26861815]

Highlights

- SPAK-inhibitor ZT-1 derivatives ameliorate post-stroke neurological function deficits
- ZT-1 derivatives ZT-1a, ZT-1c and ZT-1d improve post-stroke white/gray matter density
- ZT-1 derivatives reduce post-stroke brain lesion volume and neuronal loss
- SPAK-inhibitor ZT-1 derivatives provide a spectrum of neuroprotective effects

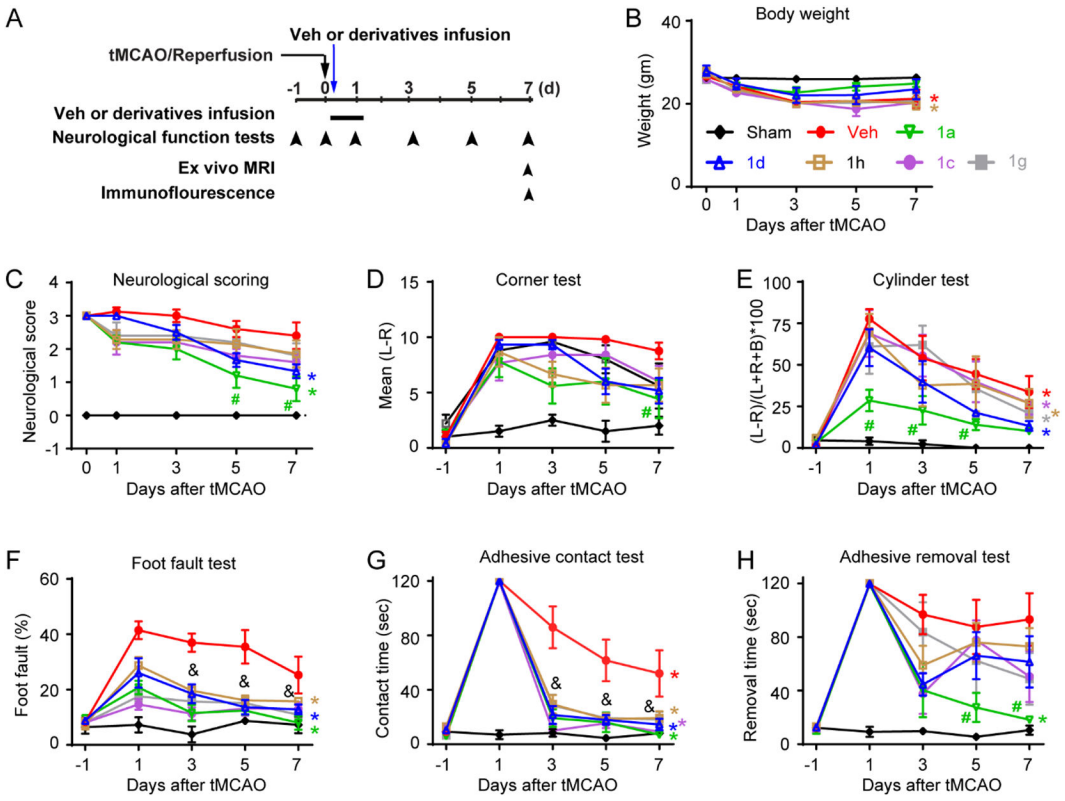

Fig. 1. Effects of ZT-1a derivatives (ZT-1c, ZT-1d, ZT-1g and ZT-1h) on neurological behavior outcome of ischemic stroke mice

(A) Experimental protocol. Sham, vehicle (Veh; 50% DMSO, 2 ml/kg) or ZT-1a and derivatives (ZT-1c, ZT-1d, ZT-1h or ZT-1g) administered with osmotic pump (5 mg/kg/day) for 3-21 hours post-MCAO. Neurobehavioral function tests were performed at pre, 0, 1, 3, 5 and 7 days post-stroke. (B) Body weight, (C) neurological scoring, (D) the corner test, (E) the cylinder test, (F) the foot fault test, (G) adhesive sensation test, and (H) adhesive removal test. Data are mean ± SEM; n = 4 (sham), 6 (veh), 5 (1a), 6 (1c), 6 (1g) and 6 (1h). $^{\&}p <$ 0.05 vs. Veh for all treatment groups; $^{\#}p < 0.05$ vs. Veh; $^{*}p < 0.05$ vs. day 1 of the treatment group.

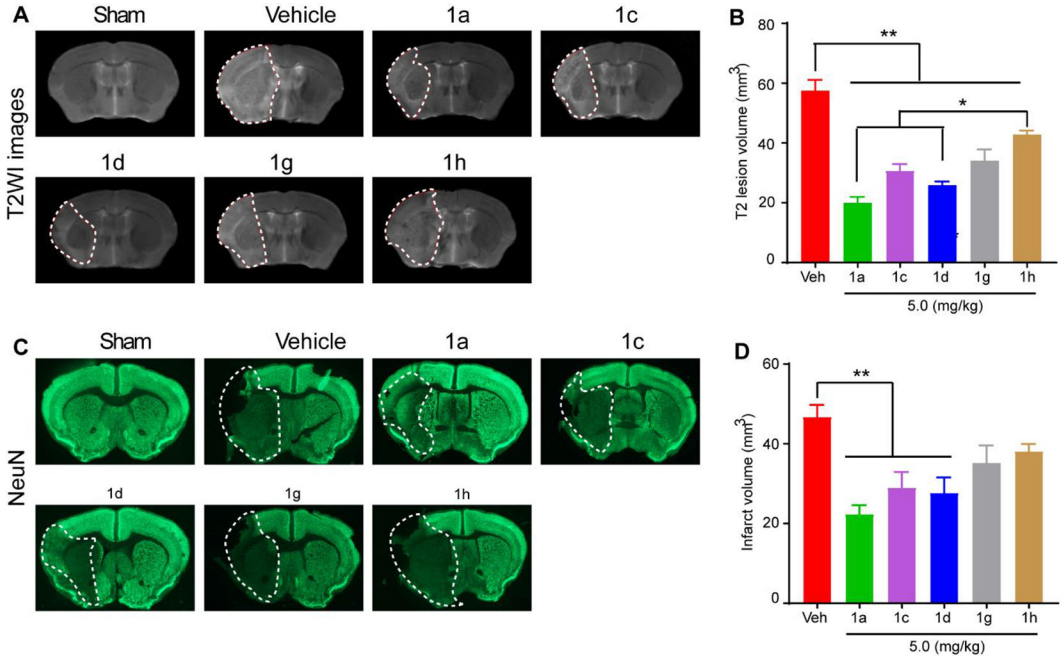

Fig. 2. Effects off ZT-1a derivatives on reducing stroke-induced infarction

(A) Representative images of MRI T2WI maps of ex vivo brains from Sham, Vehicle (Veh)-treated, ZT-1a-treated, ZT-1d-treated, and ZT-1h-treated mice at 7-day post-stroke. (B) Quantitative analysis of T2WI lesion volume in each group. Data are mean ±SEM; n = 4 (sham), 6 (veh), 5 (1a), 6 (1c), 6 (1d), 6 (1g) and 6 (1h). (C) Representative brain section images with immunofluorescence staining of NeuN. (D) Quantitative analysis of lesion volume assessed by NeuN immunofluorescence intensity. Data are mean ±SEM; n = 4 (sham), 6 (veh), 5 (1a), 6 (1c), 6 (1d), 6 (1g) and 6 (1h). *$p < 0.05$ vs. Veh; **$p < 0.01$ vs. Veh.

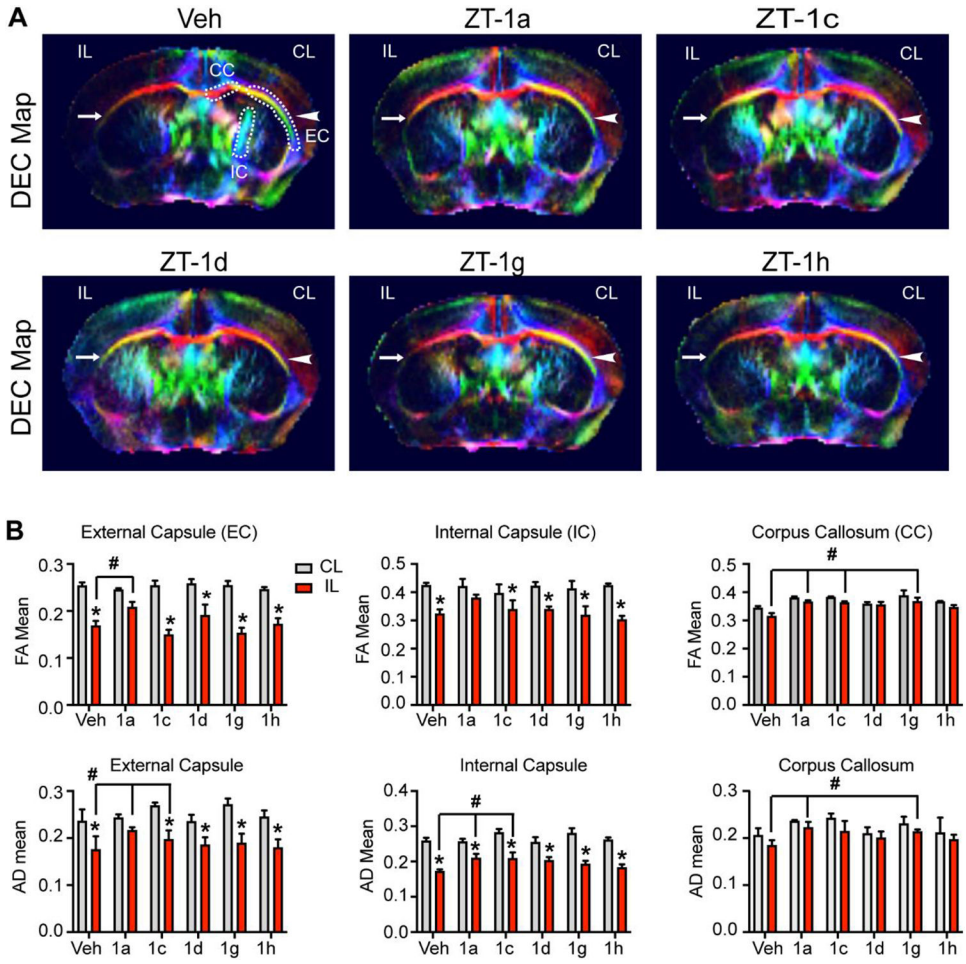

Fig. 3. Effects of ZT-1a derivatives on protecting white matter integrity of stroke brains

(A) Representative images of MRI DTI DEC maps of ex vivo brains from Veh-treated, ZT-1a-treated, ZT-1c-treated, ZT-1d-treated, ZT-1g-treated, and ZT-1h-treated mice at day 7 post-stroke, **arrowhead**: intact external capsule (EC); **arrow**: damaged EC; **dotted lines**: region of interest of EC, corpus callosum (CC), and internal capsule (IC) areas. The colors in the DEC maps represent the orientation of water diffusion, with blue indicating craniocaudal direction, red denoting right-left direction, and green indicating dorsal-ventral direction. (B) Quantitative analyses of fractional anisotropy (FA) and axial diffusivity (AD) of EC, CC, and IC. Data are mean ±SEM; n = 3 (sham), 6 (veh), 3 (1a), 3 (1c), 4 (1d), 3 (1g) and 5 (1h); $^{*}p < 0.05$ vs. CL. $^{\#}p < 0.05$ vs. Veh IL.

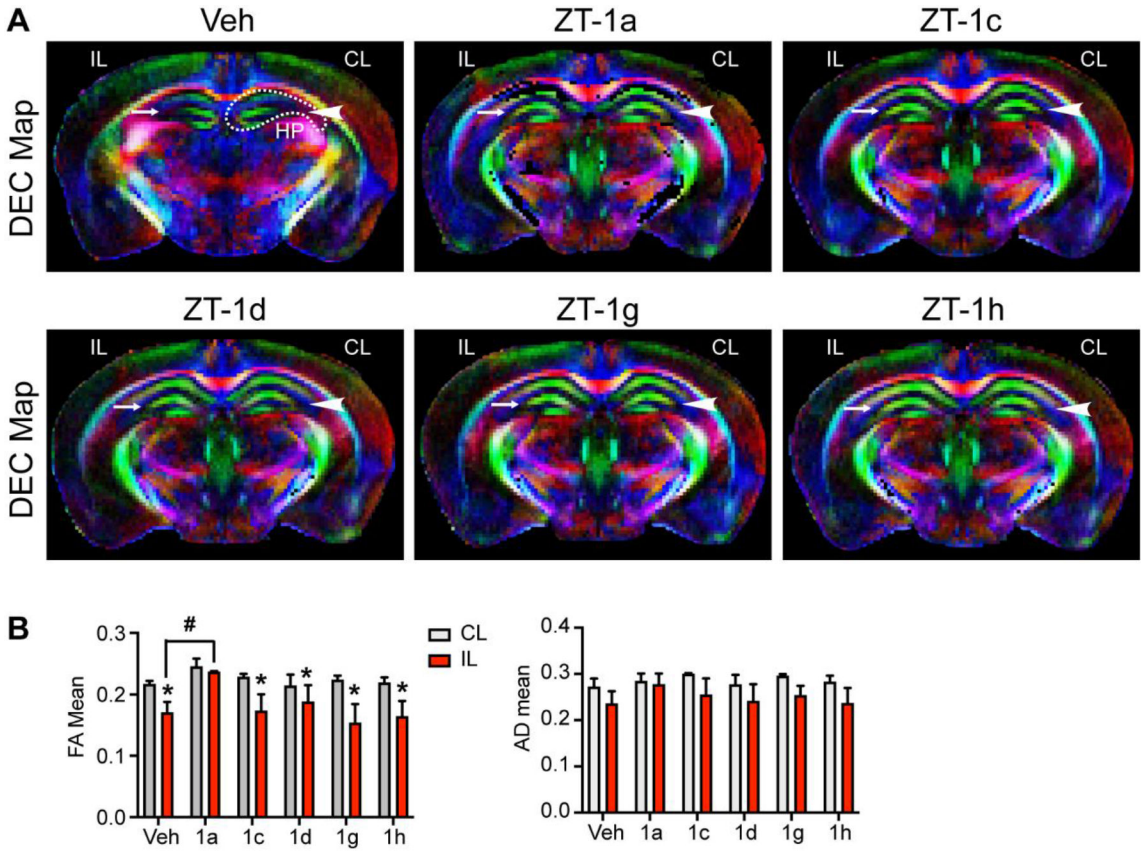

Fig. 4. Effects of ZT-1a derivatives on preserving hippocampus integrity of stroke brains.

(A) Representative images of DTI DEC maps of ex vivo brains from Veh-treated, ZT-1a-treated, ZT-1c-treated, ZT-1d-treated, ZT-1g-treated, and ZT-1h-treated mice at day 7 post-stroke. **Arrow-head**: intact hippocampus (HP); **Arrow**: damaged HP. **dotted line**: region of interest of HP. (B) Quantitative analysis of FA and AD of HP. Data are mean ±SEM; n = 3 (sham), 6 (veh), 3 (1a), 3 (1c), 4 (1d), 3 (1g) and 5 (1h); $^{*}p < 0.05$ vs. CL; $^{\#}p < 0.05$ vs. Veh IL.